J. Fluid Mech. (2005), *vol.* 524, *pp.* 305–329.
DOI: 10.1017/S0022112004002459 Printed in the United Kingdom

Elastic effects of an insoluble surfactant on the onset of two-dimensional Faraday waves: a numerical experiment

By SEBASTIÁN UBAL, MARÍA D. GIAVEDONI† AND FERNANDO A. SAITA

INTEC (Universidad Nacional del Litoral – CONICET), Güemes 3450, (3000) Santa Fe, Argentina

(Received 20 October 2003 and in revised form 15 September 2004)

The elastic effects of an insoluble surfactant on the formation and evolution of two-dimensional Faraday waves is investigated numerically. We analyse the influence of the elasticity of the surface-active agent on the amplitude of the vertical vibration needed to excite two-dimensional standing waves on the free surface. The numerical solutions show that the interface is always subharmonically excited at the onset and that the presence of the surfactant requires a higher external force to induce standing waves. They also show that the magnitude of the external amplitude is related to the temporal phase shift that exists between the evolution of the surfactant concentration and the free-surface shape. A detailed description of the time-varying velocity fields and interfacial distribution of surfactants helps to provide insight into the mechanisms ruling the phenomenon.

1. Introduction

The published studies about the conditions for the formation of waves on the surface of a liquid subject to a vertical oscillation are numerous. The phenomenon of standing waves with a frequency equal to one half the frequency of the imposed vibration was first observed by Faraday in 1831, but it was not until 1954 that Benjamin & Ursell provided a rigorous explanation of this process. These authors analysed the irrotational motion of an ideal fluid when both the amplitude of oscillation of the free surface and the liquid velocity are infinitesimally small.

A detailed review of this problem for an inviscid fluid has been given by Miles & Henderson (1990). Kumar & Tuckerman (1994) were the first to derive and solve the linear stability problem at the interface of two viscous liquids subject to a vertical acceleration. Their analysis was based on the complete fluid mechanics problem; that is, Navier–Stokes and continuity equations.

Even though the damping effects of surface-active agents on surface waves have been known for a long time (Franklin 1774), the particular topic of the role of surfactants on Faraday waves has not received much attention. When a surfactant is adsorbed at the interface, the surface tension of the free surface is lowered. In addition, if the distribution of the active solute along the free surface is not uniform, variations in surface tension will be produced. The resulting surface tension gradients exert tangential stresses at the interface, inducing flows at the free surface and in the

† Author to whom correspondence should be addressed: madelia@ceride.gov.ar

nearby liquid that transport surfactant toward regions where its concentration is lower. For the particular case of surface waves, the non-uniform distribution of a surface-active solute over the free surface is primarily due to the deformation of the interface during the oscillatory motion. Miles (1967) estimated the effects of the surfactants on the damping rates of surface waves; he also included in his analysis the viscous dissipation at the solid boundaries and the effect of the dynamic contact line formed where the free surface intercepts the lateral walls of the container. These damping rates were compared to those experimentally obtained by Henderson (1998), who also studied the effect of insoluble surfactants on the natural frequencies and amplitudes of the fundamental axisymmetric Faraday wave formed in a cylindrical container.

Recently, Kumar & Matar (2002*a*, *b*) presented two analyses of the role of insoluble surfactants in the critical oscillation amplitude required to form standing waves. In the first of these studies, they performed a linear stability analysis valid for fluids of arbitrary viscosity and depth, in which the effect of the lateral boundaries was neglected. As a consequence of the assumptions introduced, a time-independent concentration of surfactant is the only solution compatible with the existence of Marangoni flows, this solution being valid in the limit of very high Péclet number. These authors proposed that the distribution of solute presents a spatial shift with respect to the free-surface deflections and they reported solutions in which the spatial phase angle is taken as an arbitrary parameter. The main conclusion reported is that the surfactant may either raise or lower the amplitude of the external oscillation needed to produce a wavy interface depending on the value of the shift.

In the other article Kumar & Matar (2002*b*) established the magnitude of the minimum external force needed to form two-dimensional Faraday waves at the free surface of a liquid layer covered with an insoluble surfactant, when the liquid thickness is very small compared to the wavelength of the disturbance. The approach employed in their work is based on the lubrication approximation of the governing equations and the results obtained show that the contaminated liquid layer becomes more stable as the elasticity number (i.e. the ratio between the elasticity of Gibbs and the surface tension) increases; nevertheless, they predict that a clean system meeting the requirements of the approximations used cannot be excited, a result that contradicts the predictions of linear stability analysis (Kumar & Tuckerman 1994).

In the current work, we present a numerical experiment in which the influence of the Marangoni forces on the formation of two-dimensional Faraday waves is studied. The system analysed consists of a viscous liquid layer, covered with an insoluble surfactant, which is vertically vibrated at a frequency equal to 100 Hz. Thus, in the bulk phase the governing equations are Navier–Stokes and continuity with their appropriate boundary conditions. The surface-active solute modifies the interfacial stresses through surface tension; to evaluate this property – that depends on the local concentration of the surface-active agent adsorbed at the free surface – the interfacial mass balance of surfactant has to be included in the system of equations. The expression adopted here includes surface diffusion and surface convection; also, a linear relation between the surface tension and the local concentration of the adsorbed solute at the free surface is used. To the authors' knowledge, this is the first time that a solution of the complete problem is presented in the literature. Even though the predictions reported are for a particular set of quantities assigned to the governing dimensionless parameters, this set results from typical values of the physicochemical properties involved; therefore, the results depicted pertain to a representative system. The predictions obtained also provide detailed information about velocity fields and interfacial variables, which are useful for understanding the phenomena.

The numerical technique employed to achieve the solution at each time step is based on the Galerkin/finite element method combined with the parameterization of the free surface by spines and on a finite-difference predictor–corrector scheme to advance in time (Gresho, Lee & Sani 1979).

The numerical experiments are performed by first selecting a base case characterized by typical values of the physicochemical properties of a system having an inert solute at the interface. Once this case is defined, surfactant properties are considered and the external acceleration required to excite two-dimensional standing waves with a given wavenumber is numerically established for several values of the elasticity number. As the value of this parameter is raised, we found that a higher external force is involved in the formation of the standing waves. Also, the appearance of Marangoni flows due to the elastic effects gives rise to a temporal phase shift between the evolutions of the interfacial distribution of surfactant and the free surface shape. This phase shift has a size that strongly depends on the elasticity number and it can be correlated to the larger external force needed to form the waves when this parameter is augmented. We also investigate the magnitude of the phase shift in the hypothetical situation in which the diffusive transport is of the same magnitude as the convective transport; that is, when the Péclet number is 1.

The article is organized as follows. In § 2, we introduce the governing equations with the appropriate boundary conditions. Section 3 contains a brief description of the numerical methodology used to solve the set of nonlinear partial differential equations and a validation of the numerical treatment of the interfacial mass balance of surfactant. Section 4 is devoted to a discussion of the numerical solutions presented and finally, in § 5 we formulate some concluding remarks.

2. Mathematical formulation

In this work we study the formation of two-dimensional Faraday waves when the free surface of an incompressible Newtonian liquid lying on a horizontal solid plate is covered with an insoluble surfactant. The liquid layer extends on the horizontal (x, z)-plane, and its height at rest, measured along the y-coordinate, is H_0. The viscosity (μ) and density (ρ) of the liquid are constant, and the air above it is regarded as inviscid. The pressure of the gas phase is arbitrarily set equal to zero and is taken as the datum pressure.

Initially, a two-dimensional sinusoidal perturbation of amplitude εH_0 and wavenumber k is imposed on the free surface, and the temporal evolution of this disturbance is followed. The extent of the domain in the x-direction is equal to one half the wavelength of the perturbation imposed; therefore, the lateral boundaries are symmetry planes and the wavy motion developed is mirrored on both sides of this domain. Under this conditions the gas–liquid interface is described by a function of time and one space coordinate: $h(t, x)$.

The reference frame adopted is attached to the solid wall (see figure 1), which oscillates vertically with amplitude a_0 and frequency ω; therefore, the externally induced acceleration $a_0\omega^2$ is added to gravity. The equations of momentum and mass conservation are

$$\frac{\partial \boldsymbol{v}}{\partial t} + \boldsymbol{v}\cdot\nabla\boldsymbol{v} = -\nabla p + \frac{1}{Re}\nabla\cdot[\nabla\boldsymbol{v} + (\nabla\boldsymbol{v})^T] + \frac{1}{Fr}[F\cos(2\pi t) - 1]\,\boldsymbol{j}, \tag{1}$$

$$\nabla\cdot\boldsymbol{v} = 0, \tag{2}$$

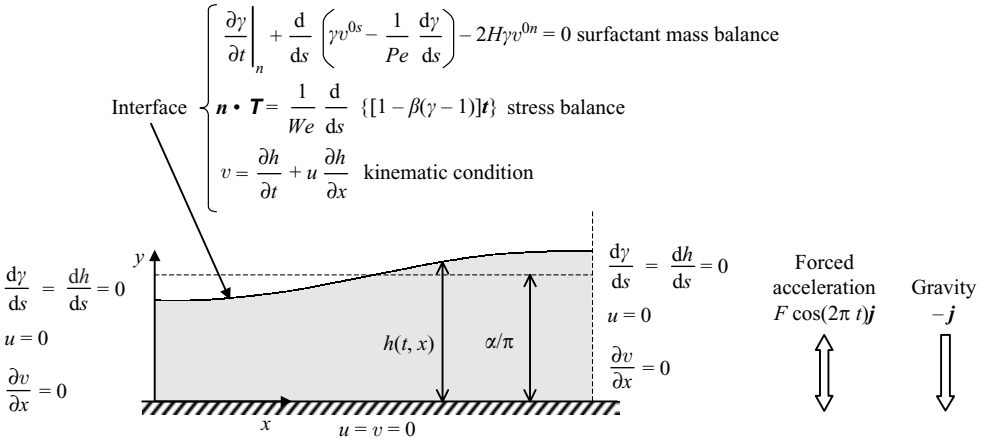

FIGURE 1. Schematic representation of the flow domain, boundary conditions and coordinate system adopted.

where $Re = \rho\omega\pi H_0^2/2\mu\alpha^2$ is the Reynolds number, $Fr = \omega^2 H_0/4\pi g\alpha$ is the Froude number, and $F = a_0\omega^2/g$ is the ratio between the external imposed force and the gravitational force. The characteristic scales adopted are $\pi/k = \pi H_0/\alpha$ for lengths, $2\pi/\omega$ for time, $\omega H_0/2\alpha$ for velocities, and $\rho(\omega H_0/2\alpha)^2$ for pressures and stresses. The initial perturbation imposed to the free surface is

$$h(t = 0, x) = \alpha/\pi[1 - \varepsilon\cos(\pi x)], \quad 0 \leqslant x \leqslant 1. \tag{3}$$

The boundary conditions required by Navier–Stokes equations are summarized in figure 1 where u and v are the x- and y-components of the velocity vector, respectively. At the bottom wall the non-slip condition is imposed while at the lateral planes, symmetry is required.

To establish the boundary conditions at the interface, we presume that the free surface is Newtonian and inviscid so that the surface stress tensor, $\boldsymbol{T}^{(S)}$, is $\boldsymbol{T}^{(S)} = \sigma(\boldsymbol{I} - \boldsymbol{nn})$, where $\boldsymbol{I}$ is the identity tensor, $\boldsymbol{n}$ is the outwardly directed unit vector normal to the interface, and σ is the gas–liquid surface tension which is a function of the amount of solute locally adsorbed; thus, the balance of stresses at the interface results:

$$\boldsymbol{n} \cdot \boldsymbol{T} = \frac{1}{We}\frac{\mathrm{d}}{\mathrm{d}s}(\overline{\sigma}\boldsymbol{t}), \quad \overline{\sigma} = \frac{\sigma}{\sigma_0}. \tag{4}$$

In equation (4), $We = \pi\rho\omega^2 H_0^3/4\alpha^3\sigma_0$ is the Weber number, σ_0 is the interfacial tension of the free surface when the concentration of surfactant corresponds to the unperturbed initial state, and $\boldsymbol{t}$ is the unit vector tangent to the free surface pointing in the direction of increasing arc-length s. If there is no surfactant adsorbed at the interface, equation (4) will simplify to the boundary condition usually imposed at a gas–liquid interface.

To evaluate expression (4) we need a functional relation connecting $\overline{\sigma}$ with the local interfacial concentration of surfactant. In this work, we assume that the deviations from the initial value σ_0 are small and, consequently, we adopt the following dimensionless linear equation:

$$\overline{\sigma} = 1 - \beta(\gamma - 1), \tag{5}$$

where, $\beta = E_0/\sigma_0$ is the elasticity number, E_0 being the Gibbs elasticity, and γ is the interfacial concentration of surfactant measured in units of its concentration at rest ($\rho_{s,0}$); hence, $\overline{\sigma}(\gamma = 1) = \sigma/\sigma_0 = 1$.

The interface is a material surface, thus the kinematic condition applies:

$$v = \frac{\partial h}{\partial t} + u\frac{\partial h}{\partial x}. \tag{6}$$

In order to evaluate (5) we must employ the interfacial mass balance of solute from which the local concentration of surfactant should be determined. For an insoluble surfactant that balance is given by (Stone 1990)

$$\left(\frac{\partial \gamma}{\partial t}\right)_n + \frac{\partial}{\partial s}\left(\gamma v^{0s} - \frac{1}{Pe}\frac{\partial \gamma}{\partial s}\right) - 2H\gamma v^{0n} = 0, \tag{7}$$

where v^{0s} and v^{0n} are the tangential and normal components of the surface velocity, H is the dimensionless curvature of the interface, $Pe = \pi\omega H_0^2/2\alpha^2 D$ is the interfacial Péclet number, D being the surface diffusivity of the surfactant, and $(\partial/\partial t)_n$ is a time derivative following the motion of the free surface along its normal direction. In (7), the second term represents transport by convection and diffusion, while the third term represents the dilution–concentration of the surfactant due to the stretching–shrinking of the free surface.

Finally, since we are interested in standing waves, symmetry boundary conditions must be satisfied at both ends of the interface, implying that $\partial\gamma/\partial s = 0$ and $\partial h/\partial s = 0$ should be imposed there.

In the next section we briefly describe the numerical technique employed to solve the complete set of governing equations and boundary conditions.

3. Numerical methodology

The nonlinear partial differential equations (1), (2), (6), and (7) with their boundary conditions were numerically solved. The technique employed is based on the finite element method and the computational mesh used follows the shape of the free surface which is obtained simultaneously with pressures, velocities and concentrations at each time step. This technique – that is basically the same as introduced by Kheshgi & Scriven (1984) to study transient free surface flows – has previously been employed by the present authors to examine the stability of a liquid layer subject to a vertical oscillation when the interface is free of surfactants (Ubal, Giavedoni & Saita 2003). Therefore, in this section we will briefly show the numerical treatment given to the interfacial mass balance of surfactant.

The structured finite element mesh consists of nine-node quadrilaterals whose form adapts to the shape of the free surface at each time step. Each element is mapped isoparametrically onto the unit square ($0 \leqslant \xi, \eta \leqslant 1$) using the nine piecewise biquadratic basis functions $\phi^k(\xi, \eta)$; with this transformation the free surface is the coordinate line $\eta = 1$.

The position of the free surface is parameterized by the distance measured along spines that are lines uniformly spaced perpendicular to the bottom wall. The shape of the gas–liquid interface is described using a quadratic interpolation of those distances. The lateral sides of the elements are spines while the upper and lower sides are located at a fixed relative distance from the interface along the spines; therefore, the elements deform following the evolution of the free surface. The flow variables are approximated by mixed interpolation: the nine biquadratic basis functions are

used for velocities, and the four bilinear ones ($\psi^l(\xi,\eta)$) for pressures. In addition, the interfacial concentration of surfactant is approximated by quadratic interpolation:

$$\gamma(\xi,t)=\sum_{i=1}^{3}\gamma^i(t)\hat{\phi}^i(\xi), \tag{8}$$

$\gamma^i(t)$ being the nodal time-dependent values of the surfactant concentration and $\hat{\phi}^i(\xi)=\phi^{i+6}(\xi,\eta=1)$ the one-dimensional specialization of the biquadratic basis functions.

The local time derivatives appearing in (1), (6), and (7) must be computed by considering the velocity of the deforming mesh; in particular the time derivative of γ (Wong, Rumschizki & Maldarelli 1996) results:

$$\left(\frac{\partial\gamma}{\partial t}\right)_n=\dot{\gamma}-\dot{\boldsymbol{x}}_{FS}\cdot\nabla_s\gamma, \tag{9}$$

where ∇_s is the surface gradient operator, $\boldsymbol{x}_{FS}$ is the free-surface location,

$$\dot{\gamma}=\left(\frac{\partial\gamma}{\partial t}\right)_\xi=\sum_{i=1}^{3}\frac{\mathrm{d}\gamma^i}{\mathrm{d}t}\hat{\phi}^i(\xi),\ \text{and}\ \dot{\boldsymbol{x}}_{FS}=\left(\frac{\partial\boldsymbol{x}_{FS}}{\partial t}\right)_\xi=\boldsymbol{j}\sum_{i=1}^{3}\frac{\mathrm{d}h^i}{\mathrm{d}t}\hat{\phi}^i(\xi).$$

The Galerkin/finite element method employed requires constructing the weighted residuals of (1), (2), (6), and (7) in order to obtain a set of nonlinear ordinary differential equations. For example, once the term affected by $\mathrm{d}/\mathrm{d}s$ has been integrated by parts, the residual of the interfacial mass balance of solute (7) may be written as

$$R_S^i=\int_{FS}\left\{\hat{\phi}^i[\dot{\gamma}-\dot{\boldsymbol{x}}_{FS}\cdot\nabla_s\gamma-2H\gamma v^{0n}]-\frac{\mathrm{d}\hat{\phi}^i}{\mathrm{d}s}\left(\gamma v^{0s}-\frac{1}{Pe}\frac{\mathrm{d}\gamma}{\mathrm{d}s}\right)\right\}\mathrm{d}s$$
$$-\left[\gamma v^{0s}-\frac{1}{Pe}\frac{\mathrm{d}\gamma}{\mathrm{d}s}\right]_{x=0}^{x=1}=0,\quad i=1\ldots NF, \tag{10}$$

where NF is the number of nodes located along the free surface.

The resulting set of ordinary differential equations is discretized in time using a finite difference predictor–corrector scheme. The time derivatives are approximated with the trapezoidal rule, and the final set of nonlinear algebraic equation is solved using a Newton loop. An Adams–Bashforth predictor provides a first estimation of the solution and enhances the convergence of the iterative process. The size of the time step is controlled according to Crisfield's method in order to meet the convergence criterion adopted (the mean square root of the error in the Newton loop must be smaller than 10^{-6}) in a predetermined number of iterations. Thus, we have

$$\Delta t_n=\Delta t_{n-1}\left(\frac{DNIT}{NIT_n}\right),\quad \Delta t_n=t_{n+1}-t_n,\quad DNIT=3, \tag{11}$$

where t_{n+1} and t_n represent the time at the present $(n+1)$ and previous (n) time steps, respectively, NIT_n accounts for the number of iterations effectively required to meet the convergence criterion in the previous time step while $DNIT$ is the number of iterations sought. In addition, the size of the time step cannot be larger than 0.02. If the convergence criterion is not met, the solution at time step $n+1$ is recomputed with a Δt equal to one half the value of the Δt previously used.

3.1. *Selection of the mesh and numerical tests*

The criteria followed to determine the appropriate finite element mesh were the following:

(i) There is one boundary layer near the free surface and another one just above the solid walls; consequently, the mesh is refined in these regions.

(ii) Numerical oscillations in the surfactant concentration at high Péclet numbers should be negligible.

(iii) Errors in the surfactant mass balance due to the quadratic interpolation functions employed should be bounded to a small amount, typically the cumulative error between the first and the last time step of a simulation is less than 2%.

The last criterion results from the following numerical test: we computed the evolution of a system represented by typical values of the dimensionless parameters using three different finite element meshes. In this test, the values employed were $\alpha = 1.26$, $\alpha^2\ Re = 39.478$, $\alpha^3\ We = 5.6375$, $\alpha\ Fr = 3.206$, $\alpha^2\ Pe = 394784$, $F = 15$, $\beta = 0.2$, and the meshes tested had 70, 105 and 140 elements. To determine the cumulative error in the mass balance of solute, we recorded the total amount of surfactant absorbed at the interface at each time step ($m_\gamma(t_n)$) and we evaluated the expression

$$\frac{m_\gamma(t_n) - m_\gamma(t=0)}{m_\gamma(t=0)} \times 100.$$

The error thus computed was equal to 2.8%, 1.3% and 0.7%, when the number of elements of the mesh was 70, 105 and 140, respectively.

In order to detect the differences in the solutions associated with the three tessellations and, consequently, to the error in the mass balance we followed the time evolution of the interfacial area per unit width and the departure of the surfactant concentration from its equilibrium value at $x = 0$. The first was chosen because it shows the global changes experienced by the interfacial shape while the second was selected because it is representative of the modifications experienced by any of the interfacial variables. The plot of the time evolution of these quantities presented in figure 2 indicates that the three solutions are qualitatively similar. Thus, we conclude that an error in the mass balance no larger than 2% is sufficient to accurately describe the evolution of the system.

A detailed description of the numerical tests carried out in order to determine a finite element mesh that fulfils all the criteria listed at the beginning of this section is presented elsewhere (Ubal 2002). From these experiments, a mesh of 140 elements was found appropriate to follow the evolution of the free surface and the interfacial concentration of surfactant in almost all the cases considered in this work. In a few cases a more refined mesh was used.

The numerical methodology employed here has previously been used to solve the problem for pure liquids (Ubal *et al.* 2003) and the solutions obtained were in excellent agreement with the viscous linear theory reported by Kumar & Tuckerman (1994). Therefore, the numerical validations presented here are related to the effects produced by the surface-active agent only.

As mentioned in the Introduction, the literature specifically addressing the influence of surface-active agents on Faraday waves is not very extensive (Henderson 1998; Kumar & Matar 2002*a*, *b*); moreover, the experiments of Henderson are in a cylindrical container, and the analytical works by Kumar & Matar are either for very long disturbances in a very thin film – a situation not appropriate for numerical experiments due to the large computational time required – or for the especial case in which the

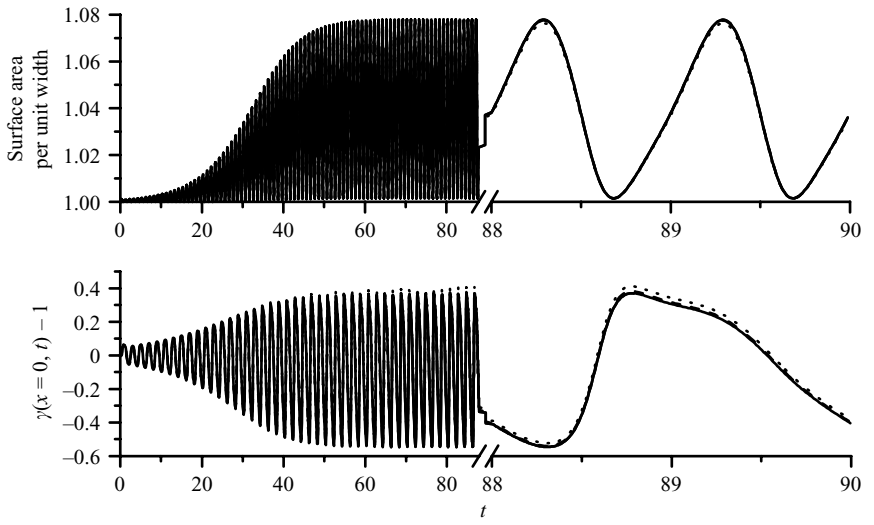

FIGURE 2. Interfacial area per unit width and surfactant concentration deviation from equilibrium at $x = 0$ versus time computed with a mesh having: . . . ., 70 elements; - - - -, 105 elements; —, 140 elements. The parameters of the system are $\alpha = 1.26$, $\alpha^2 Re = 39.478$, $\alpha^3 We = 5.6375$, $\alpha Fr = 3.206$, $\alpha^2 Pe = 394784$, $F = 15$, and $\beta = 0.2$.

distribution of surfactant is time independent. Consequently, a comparison of our numerical solutions with the results of those works is not suitable.

A problem that can be used to test the numerical code is the analysis of the free oscillations carried out by Miles (1967). This author presented a weakly nonlinear analysis in which approximate analytical expressions for the damping coefficients of surface waves under the influence of surface-active agents were developed. For the geometry analysed here these expressions are as follows:

$$\delta = \delta_b + \delta_s, \delta_b = \frac{kd\omega_N}{2\sinh(2kH_0)}, \quad \delta_s = \frac{1}{4}kd\omega_N \left[\frac{\varsigma^2}{(\zeta-1)^2+1}\right] \coth(kH_0), \tag{12}$$

where δ_b and δ_s are the contributions to the damping rate of the viscous dissipation that occurs in the boundary layer existing on the solid wall, and the damping induced by the elastic effect of an insoluble surfactant adsorbed at the free surface, respectively. In (12), $d = \sqrt{2\nu/\omega_N}$ is the Stokes boundary layer thickness, ν is the kinematic viscosity, $\omega_N = \sqrt{(gk + \sigma_0 k^3/\rho)\tanh(kH_0)}$ is the natural frequency corresponding to an inviscid oscillation, and $\varsigma = (k^2 E_0/\rho)\sqrt{2/\nu\omega_N^3}$. This analysis is based on the assumption that both kd and d/H_0 are much smaller than one.

To validate our method, numerical tests were done in which the damping coefficient for different values of the Gibbs elasticity (E_0) was evaluated and compared with the coefficient calculated with (12). The initial perturbation (3) with $\varepsilon = 0.15$ is imposed at the free surface at the beginning of the simulations; the physicochemical and geometrical properties of the system being as follows: $\rho = 1000\,\mathrm{kg\,m^{-3}}$, $D = 2.5 \times 10^{-9}\,\mathrm{m^2\,s^{-1}}$, $\sigma_0 = 0.055\,\mathrm{Nm^{-1}}$, $H_0 = 10^{-3}\,\mathrm{m}$, $k = 1260\,\mathrm{m^{-1}}$, $\mu = 0.001\,\mathrm{Pa\,s}$. Therefore, $d = 7.87 \times 10^{-5}\,\mathrm{m}$ and $kd \sim 0.1$ and $d/H_0 \sim 0.08$; that is, a situation in which the hypotheses invoked by Miles are fairly well satisfied. Even though the analysis of Miles is applicable to disturbances of very small amplitude, Henderson (1998) has experimentally verified that equation (12) is still valid when the slope of the waves is larger than one; therefore, fixing ε at 0.15 is appropriate.

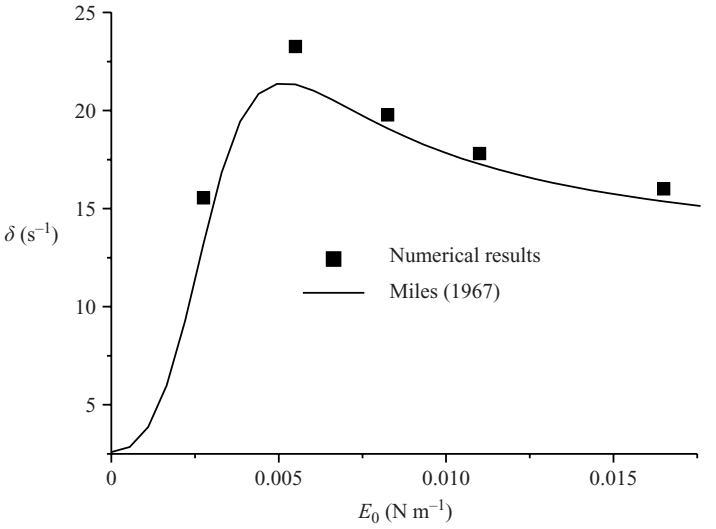

FIGURE 3. Damping coefficients of surface waves under the influence of surfactants. Approximate analytical solution of Miles (1967) and prediction from the present numerical solution. The physicochemical and geometrical properties of the system are as follows: $\rho = 10^3$ kg m^{-3}, $D = 2.5 \times 10^{-9}$ m^2 s^{-1}, $\sigma_0 = 0.055$ N m^{-1}, $H_0 = 10^{-3}$ m, $k = 1260$ m^{-1}, $\mu = 10^{-3}$ Pa s.

The numerical damping coefficient was obtained as follows. Once the initial sinusoidal perturbation is imposed, the free surface presents an oscillatory behaviour that decays in time in an approximately exponential mode. We detected the local maxima of the amplitude of the free-surface oscillation at $x = 0$ for $t \geqslant 0$, and we evaluated the function

$$g(t) \equiv \ln \left\{ \text{abs} \left[\frac{h(t, x = 0)}{\alpha/\pi} - 1 \right] \Big/ \varepsilon \right\}$$

for at least 10 oscillations of the free surface. These values were fitted to the best linear approximation using standard minimum-squares, the slope of the straight line thus obtained being the numerical damping coefficient of the oscillation.

In figure 3 we depict the analytical and numerical values of the damping coefficients as a function of E_0. It can be observed that both the numerical and analytical predictions are very close, as expected. In his analysis, Miles neglected viscous dissipation in the bulk under the assumption that the boundary layer thickness is small compared to the fluid depth; therefore, the small differences observed between the numerical and the analytical coefficients can be attributed to this approximation.

4. Results

As we stated in the Introduction, the main goal of this work is to investigate the effects of insoluble surfactants on two-dimensional Faraday waves by means of the direct numerical solution of the governing equations described in § 2. In particular, the influence of the elasticity number on the stability of the system was analysed. To this end, the evolution of several flow variables for selected values of β was carefully examined in order to provide further insight regarding the formation of the waves.

The investigation was carried out for a particular set of dimensionless parameters,

$$\alpha^2 \, Re = 39.478, \quad \alpha^3 We = 5.6375, \quad \alpha Fr = 3.206, \quad \alpha^2 Pe = 394784$$

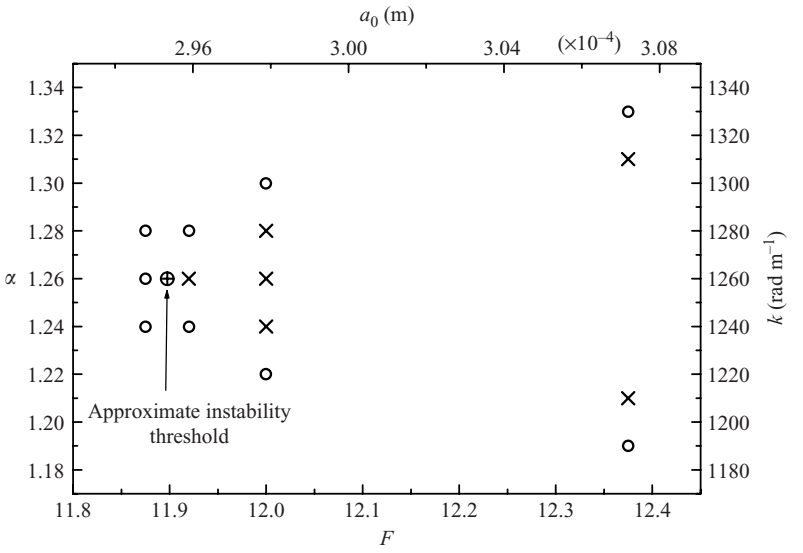

FIGURE 4. Stability map corresponding to the reference set (RS), $\alpha = 1.26$, and $\beta = 0$. Crosses denote unstable solutions (the initial amplitude imposed on the free surface increases with time) and circles stable ones (the initial amplitude imposed on the free surface decays to zero). RS is defined by the following set of dimensionless parameters: $\alpha^2 Re = 39.478$, $\alpha^2 We = 5.6375$, $\alpha Fr = 3.206$, $\alpha^2 Pe = 394784$, $F = 15$.

which will be identified as the reference set (RS) and corresponds to the following typical values of the physical variables:

$$\rho = 1000\,\mathrm{kg\,m^{-3}}, \quad \mu = 0.025\,\mathrm{Pa\,s}, \quad D = 2.5 \times 10^{-9}\,\mathrm{m^2\,s^{-1}},$$
$$\sigma_0 = 0.055\,\mathrm{N\,m^{-1}}, \quad H_0 = 10^{-3}\,\mathrm{m}, \quad \omega = 200\pi\,\mathrm{s^{-1}}.$$

The numerical solutions presented in this Section are organized as follows. First, we select a particular value of the wavenumber (α) in order to completely define a reference case for the numerical experiments. Then, we analyse the influence of the elasticity number on the critical vibration amplitude required to produce waves of wavenumber α. The flow fields associated with the standing waves formed for selected values of β are discussed next. Finally, we briefly report the changes experienced by the system when the Péclet number is largely reduced.

4.1. *Selection of the reference case*

In order to analyse the effects of the elasticity on the development of the instability, we choose a reference case. This case results from a stability analysis of the system when the elasticity of the film is zero ($\beta = 0$, or $E_0 = 0$), that is, the solute adsorbed at the interface is not a surfactant, and the other dimensionless numbers take the values previously mentioned. Under these conditions, there exists a particular wavenumber ($\alpha = \alpha_C$) that requires a minimum excitation amplitude ($F = F_C$) to form a wavy motion. A stability map in the (F, α)-plane was constructed in order to numerically determine this critical point, and the resulting chart is shown in figure 4. Every cross and circle in this graph represents the outcome of a single simulation that is started with the liquid at rest, a uniform concentration of surfactant ($\gamma = 1/S_0$, being S_0 the initial interfacial length of the surface), and the free surface slightly perturbed from the horizontal flat state, according to (3) with $\varepsilon = 0.05$.

In figure 4, crosses denote unstable results, while circles indicate stable outcomes. The criterion adopted for this classification is the following: when the amplitude of the oscillation initially imposed on the free surface decays to zero, the numerical experiment is considered stable; otherwise the simulation is catalogued as unstable. The unstable cases shown are characterized by subharmonic oscillations of standing waves whose wavelengths are double the horizontal dimension of the computational domain. The point marked with $\oplus$ ($F_C = 11.9$, $\alpha_C = 1.26$) represents the approximate critical conditions for wave generation and it will be regarded as the reference case in the numerical experiments presented in this work. As we expected, the predicted value for α_C is somewhat larger than that predicted by the dispersion relationship of the inviscid linear theory (Benjamin & Ursell 1954): $\alpha_C \sim 1.239$.

4.2. *Effect of the elasticity number on the stability of the system*

The damping effect of adsorbed films on surface waves has been known for a long time (see e.g. Franklin 1774; Lamb 1945). The basic mechanism of action is also well known, and it can be summarized as follows.

When a wavy motion is established and the Péclet number is large, the liquid moving from the valley towards the crest of a wave convects the adsorbed surfactant to this region, and if the dilution of the solute due to the interfacial deformation is not too large a positive concentration gradient directed from the trough toward the crest of the wave will be established. This gradient gives rise to a non-zero tangential component of the traction vector along the interface, pointing toward the region of larger interfacial tension (lower concentration of surfactant). These tensions – that are known as Marangoni tensions – try to restore a uniform distribution of surfactant by pulling the interface in the opposite direction to the motion of the bulk, in this way damping the surface waves.

If the magnitude of the Marangoni effect is large enough, there will be an interfacial backflow that carries surfactant from the crest to the trough of the wave during part of the cycle in which the flow in the liquid phase is still driving fluid toward the crest; therefore, there will be a temporal phase shift between the cycle experienced by the distribution of surfactant along the interface and the cycle corresponding to the free-surface shape. The temporal phase angle between the two evolutions depends on the particular set of values of the dimensionless parameters that characterize the system.

In a recent work, Kumar & Matar (2002*a*) considered the Faraday-wave problem for a viscoelastic liquid covered by an insoluble surfactant. They conducted a linear stability analysis of the governing equations for the bulk phase (momentum and mass balance), and the interface (momentum and surfactant mass balance), that allowed them to construct neutral stability curves in the wavenumber vs. excitation-amplitude plane. However, it is important to note that in their analysis – valid in the limit of very large Pe – the interfacial mass-balance of the surface-active solute reduces to $\partial\gamma/\partial t = 0$. Kumar & Matar assumed that the resulting time-independent distribution of surfactant presents a certain spatial phase shift with respect to the surface deflection. This phase shift is considered as an arbitrary parameter in their model. We will show that a temporal phase shift does appear between the distribution of surfactant and the free-surface deflection, and that this temporal phase shift strongly depends on the elasticity number.

In order to examine the influence of the elasticity of the surfactants on the stability of the system, we numerically determined the minimum driving force F needed to develop surface standing waves for several values of the parameter β; the wavenumber

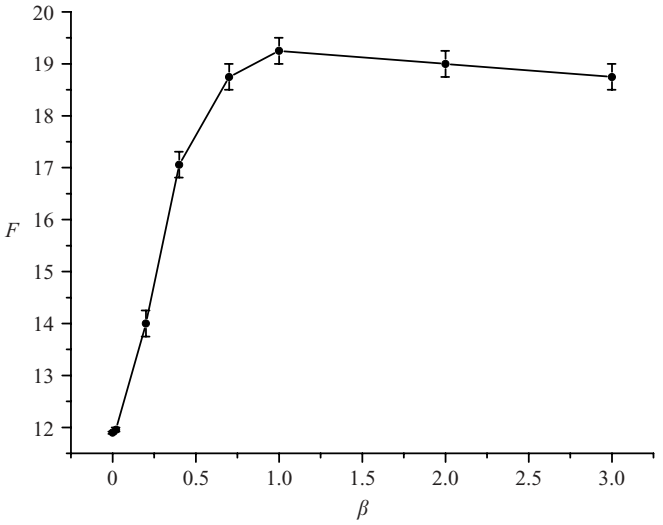

FIGURE 5. Minimum dimensionless excitation force needed to form waves with wavenumber $\alpha = 1.26$ versus β. The parameters of the system have the same values as in RS (see the caption of figure 4). The bars represent the numerical uncertainty in the computed minimum values of F.

adopted for this set of numerical experiments was $\alpha = 1.26$, the 'optimal' when the elasticity of the adsorbed film is zero. The results obtained are summarized in figure 5, where the bars represent the numerical uncertainty in the computed minimum values of F. That is, each point is located between the maximum F at which a stable solution was obtained and the minimum F at which an unstable solution was computed.

It can easily be verified that the threshold forcing amplitudes are larger for non-zero values of the elasticity number than for the base case ($\beta = 0$); that is, the system tends to become more stable as β becomes larger. However, the critical driving force does not increase monotonically with β. Results illustrated in figure 5 show that F increases rapidly with an increase of β until a maximum is reached near $\beta = 1$, and from this point on F slowly diminishes.

Next, we analyse the evolution of the interfacial variables for selected values of β in order to gain more insight into the results described above.

4.3. *Evolution of the interfacial variables for different values of* β

In this section we examine the time evolution of the maximum absolute value of the tangential and normal components of the velocity and traction vectors along the interface (v^{0s}, v^{0n}, T_{nt}, T_{nn}), the surfactant concentration deviation ($\gamma - 1$) and free-surface location (h) at the left and right ends of the computational domain. The analysis is carried out near the threshold ($F = 14.25$, 19, 19.5, and 19, respectively) when $\alpha = 1.26$, for four values of the parameter β (0.2, 0.7, 1 and 3).

In all the experiments performed, the magnitude of any of these variables increases from its initial value until a stationary oscillatory state is developed, in which the motion of the free surface is subharmonic and the amplitude of the oscillation is almost independent of β. Numerical results for $\beta < 0.2$, not presented here, show that the elastic effects are very weak, the temporal evolution of v^{0s}, v^{0n}, and T_{nn}, being comparable to the time-evolution presented by these variables in a system with $\beta = 0$.

They also show the values of T_{nt} to increase with β as expected, but they are still small enough to have a significant effect on v^{0s}. On the other hand, if β is larger than approximately 0.2, the time-evolution of some of the interfacial variables is very sensitive to this parameter; this feature is shown in figures 6–9 where the results corresponding to the selected values of the elasticity number are depicted.

In those figures, dashed lines are used to indicate either negative values of v^{0s} and T_{nt}, or the values taken by v^{0n} and T_{nn} during the part of the cycle in which either the liquid in the bulk moves from $x=1$ to $x=0$ or the normal stresses try to force a motion from the right to the left.

Since the cases studied are near the stability limit, the oscillation of the free surface (figures 6*f*–9*f*) has a similar amplitude in all of them. Consequently, the magnitude of both v^{0n} and T_{nn}, which are closely related to the oscillation amplitude, also presents relatively similar values (see figures 6*a*, *c*–9*a*, *c*). These results suggest that the term $2H\gamma v^{0n}$ in (7) representing the dilution/concentration of the surfactant due to the deformation of the free surface during its cyclic motion has a similar influence on the local concentration of solute in all the examples considered, as we will confirm later with the results to be shown in figure 13.

A totally different situation is observed for the maximum magnitude of the tangential component of the surface traction (figures 6*d*–9*d*), as well as for the tangential interfacial velocity (figures 6*b*–9*b*), and for the departure of the surfactant concentration from its equilibrium value at the ends of the domain (figures 6*e*–9*e*); all these variables are clearly affected when the elasticity number (β) is changed. As β is increased, the Marangoni stresses increase, even though the concentration gradients tend to diminish as we will show later. These stresses reduce the magnitude of the tangential component of the interfacial velocity in an attempt to minimize the surface tension gradients inducing the appearance of a temporal phase shift between the motion along the free surface and the motion of the liquid in the bulk (see figures 6*b*–9*b* and 6*f*–9*f*). This phase shift can easily be detected by comparing the curves of $h(t,0)$ (or $h(t,1)$) and $\max|v^{0s}|$; in fact, the time evolution of these variables shows that the interfacial velocity turns backward before the reversal of the liquid motion in the bulk takes place (the time at which the maximum height is achieved by the liquid at $x=0$ does not agree with the instant at which $\max|v^{0s}|$ is almost zero). In the present case, due to the large value of the Péclet number ($Pe \approx 248\,667$), the surfactant is transported mostly by convection and the local concentration of solute evolves ahead of the free-surface deflections (see figure 6*e*–9*e* and 6*f*–9*f*). As we will show later in figure 13, the magnitude of this transport diminishes when the elasticity number is increased, producing a more uniform distribution of the solute along the interface and thus affecting the magnitude of the elastic effects ($\mathrm{d}\overline{\sigma}/\mathrm{d}s$).

Another feature shown by figures 6(*b*)–9(*b*) is the remarkable change in the pattern of the tangential component of the surface velocity associated with variations of the elasticity number. In fact, the results illustrated in figures 8(*b*) and 9(*b*) show that the tangential velocity changes sign more than once during the cycle, pointing out the existence of swirling flows near the interface. This phenomenon will be more carefully examined in § 4.4.

According to the curves depicted in figures 8(*d*) and 9(*d*) the tangential component of the traction vector is slightly modified when the elasticity number is varied between 1 and 3. Thus, the main effect of the surfactant within this range of β is to produce a drastic reduction of the magnitude of v^{0s} (see figures 8*b* and 9*b*) and consequently, a remarkable reduction in the departure of the interfacial concentration of surfactant from its concentration at rest (see figures 8*e* and 9*e*).

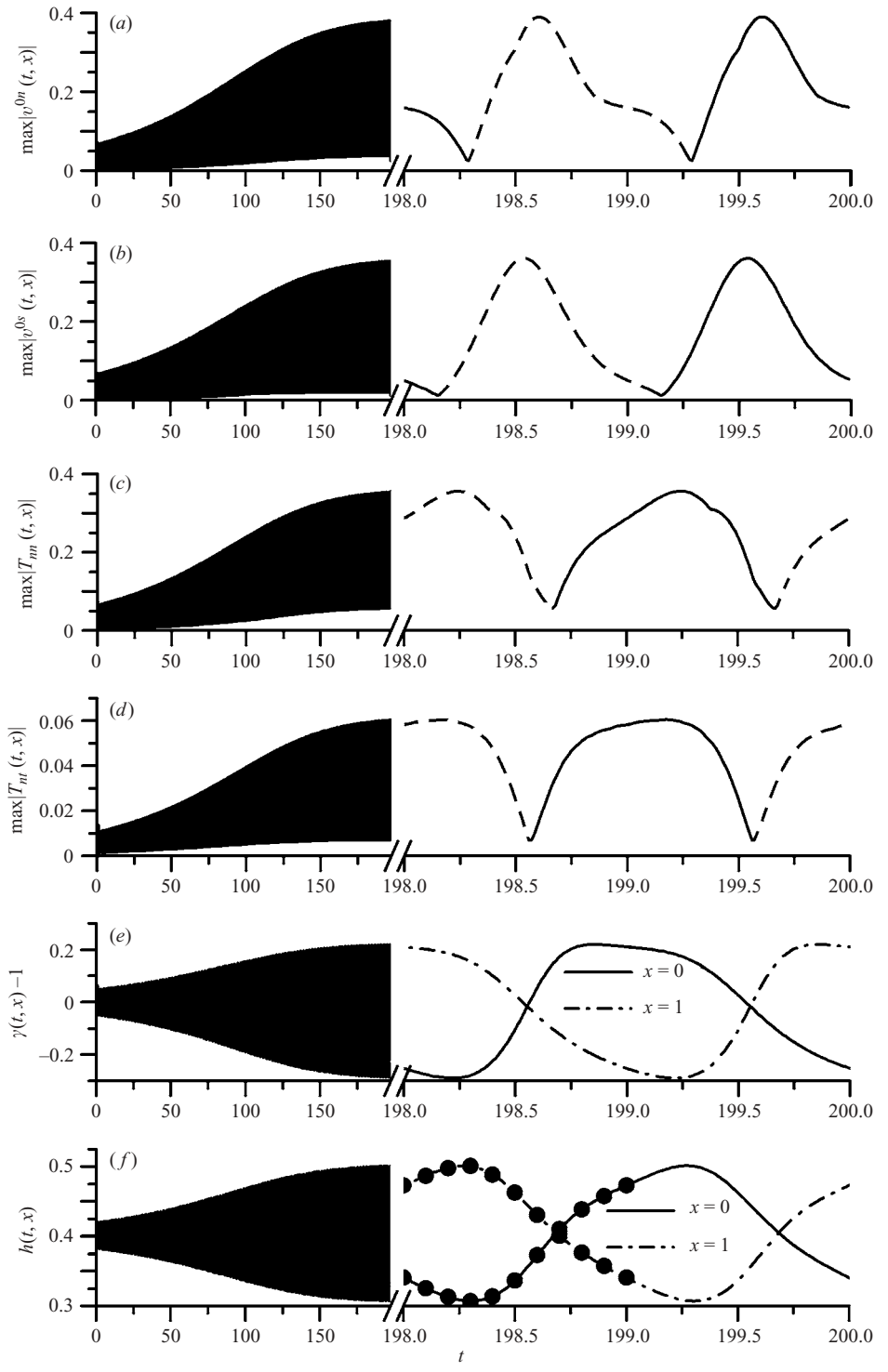

FIGURE 6. Time evolution of several interfacial variables for RS, $\alpha = 1.26$, $\beta = 0.2$, $F = 14.25$. (*a–d*) maximum absolute values of normal and tangential components of both surface velocity and interfacial traction, (*e*) surfactant concentration deviation from equilibrium, and (*f*) free-surface position at both ends of the computational domain. The dots in (*f*) identify the state of the system whose streamlines are shown in figure 11(*a*).

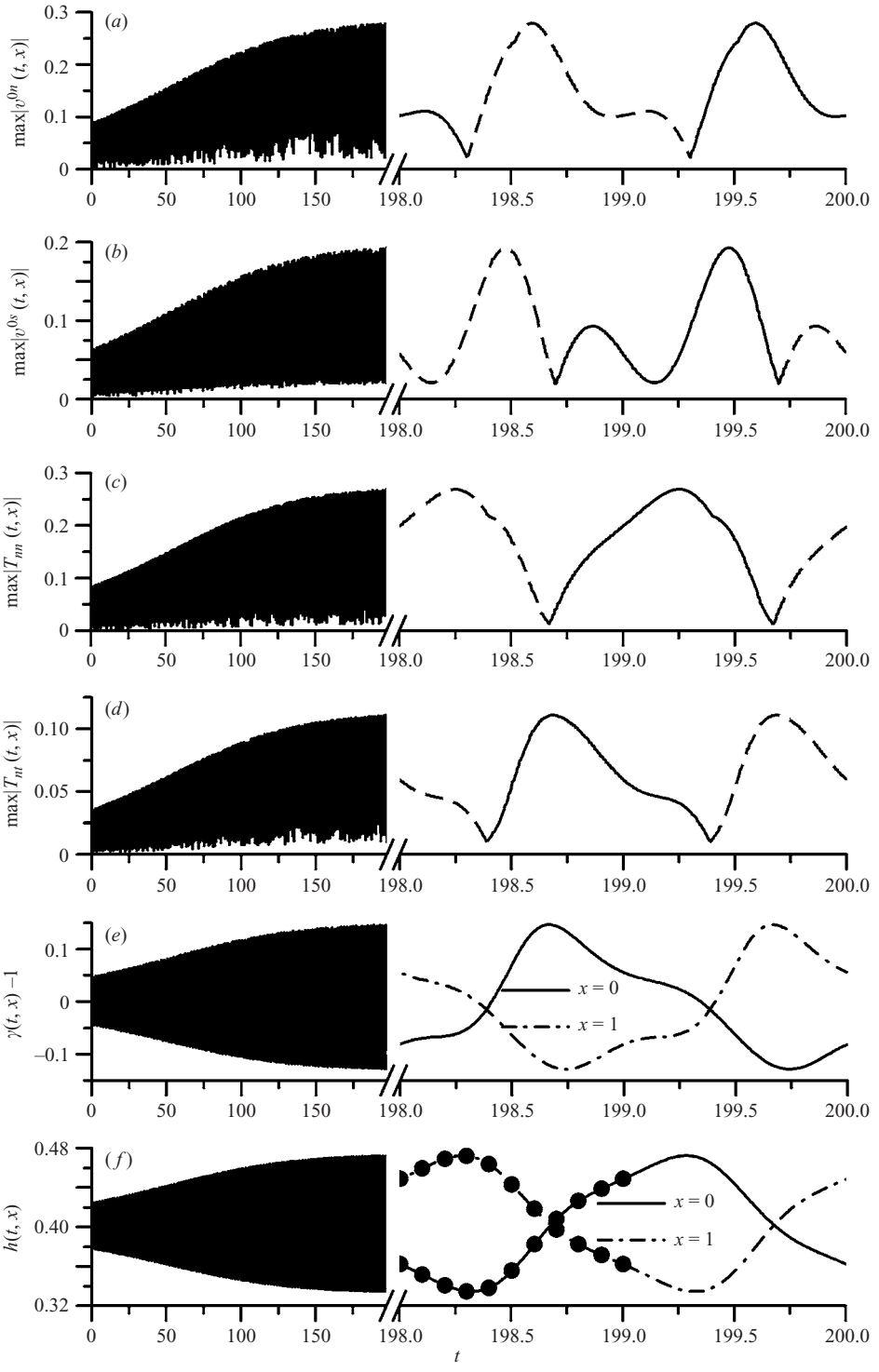

FIGURE 7. As figure 6 but for $\beta = 0.7$, $F = 19$.

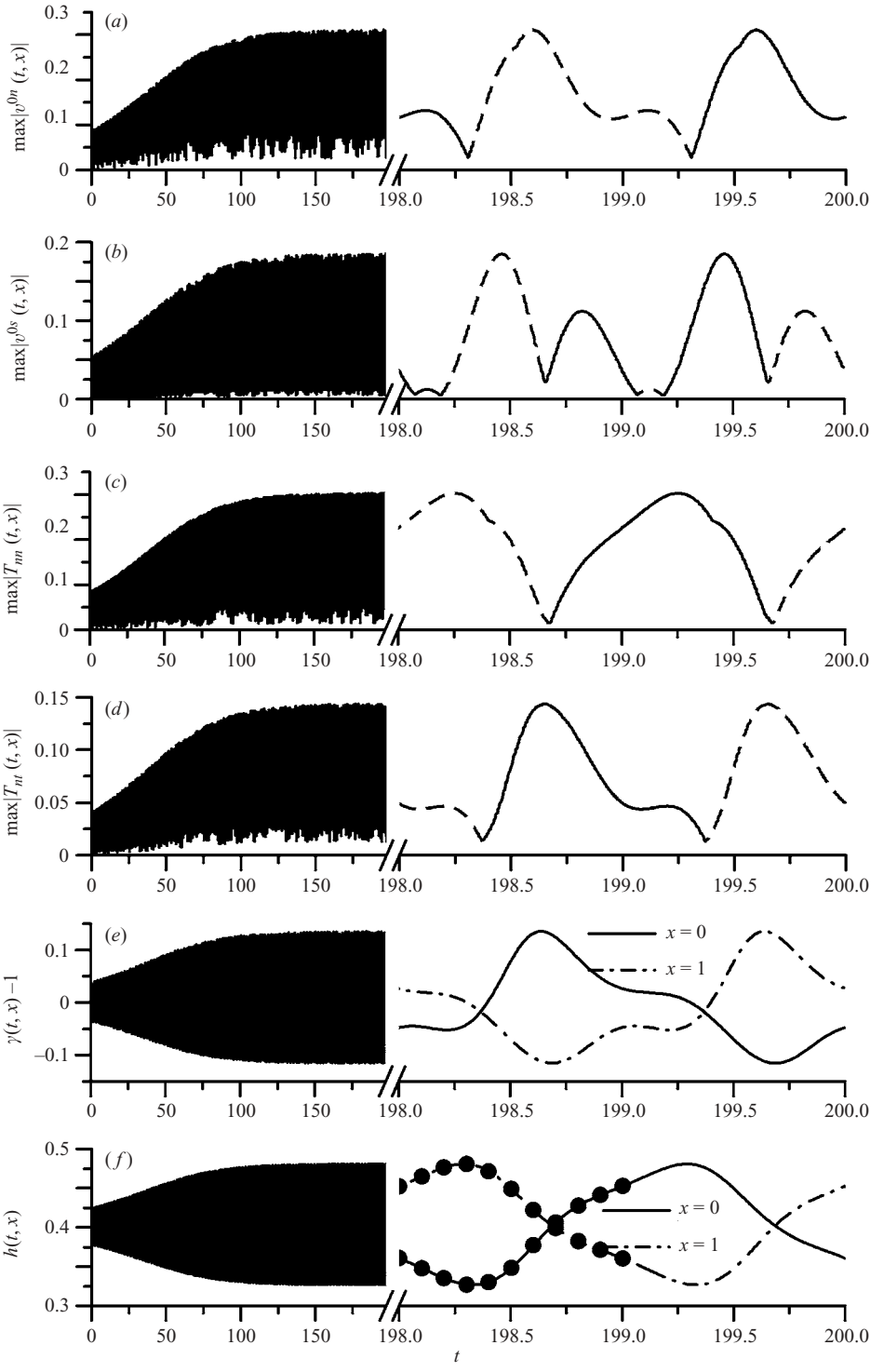

FIGURE 8. As figure 6 but for $\beta = 1$, $F = 19.5$. The dots in (f) identify the state of the system whose streamlines are shown in figure 11(b).

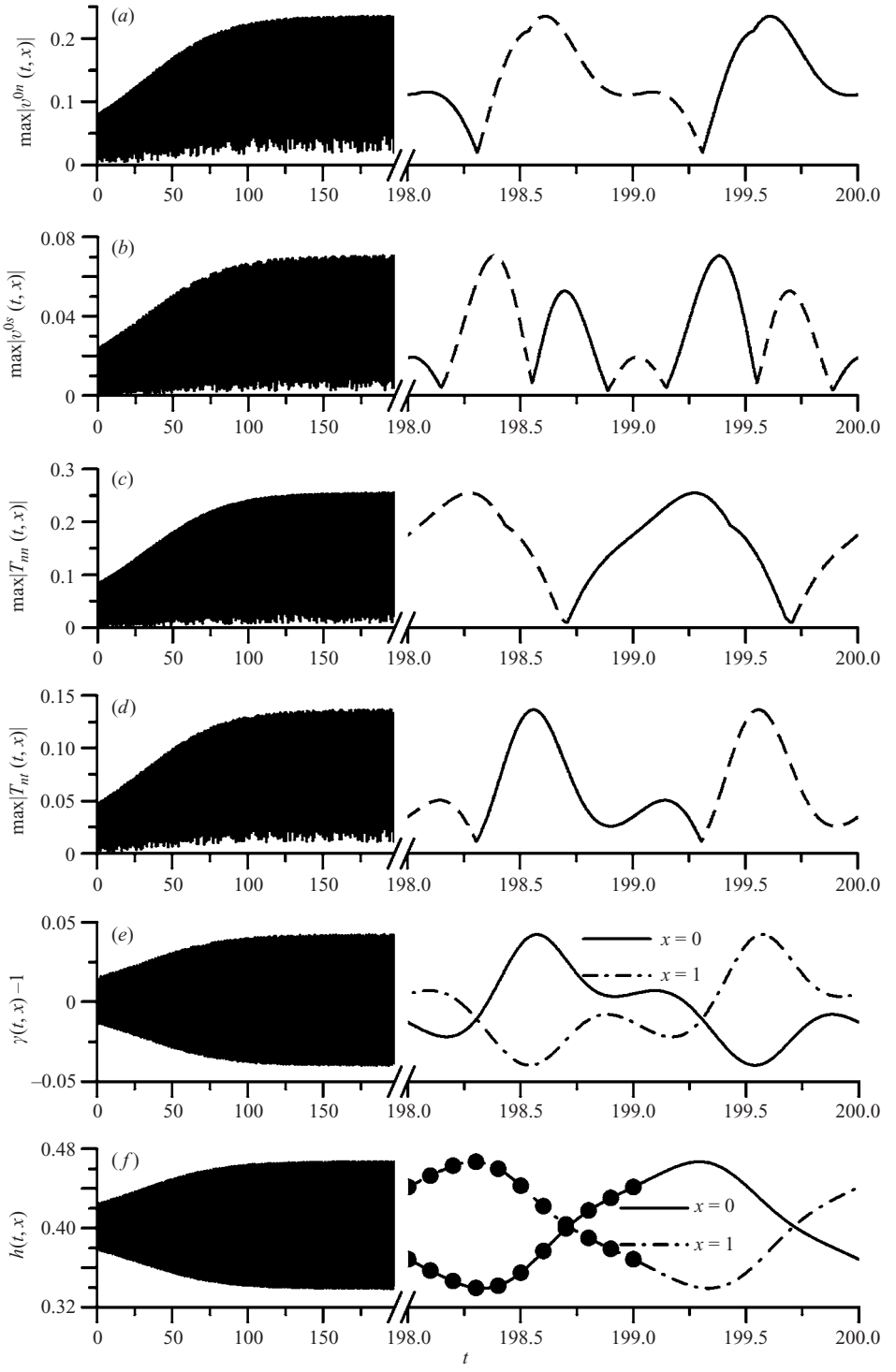

FIGURE 9. As figure 6 but for $\beta = 3$, $F = 19$. The dots in (f) identify the states of the system whose streamlines are shown in figure 11(c).

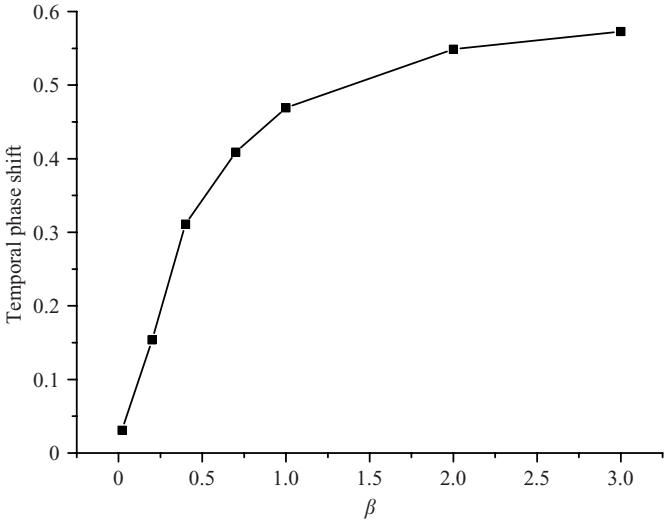

FIGURE 10. Influence of the elasticity number on the temporal phase shift at $x = 0$ between the surfactant concentration and the free-surface location. The parameters of the system are those of RS (see the caption of figure 4) and $\alpha = 1.26$.

The force F required to form a wavy motion strongly depends on the elasticity number; we have previously pointed out in this section that when β increases there will be a larger temporal phase shift between the evolution of the free-surface deflections and the evolutions of both the local concentration of surfactant and the tangential surface velocity. The Marangoni tractions associated with this shift pull the interface and the surrounding liquid against the direction of motion of the bulk, retarding the appearance of the waves and increasing the amplitude of the external acceleration needed to form them. Therefore, the phase shift might be associated with the forcing acceleration and one could expect that the curves of $F$and the phase shift versus β will present similar trends.

Results reported in figures 6(e, f) – 9(e, f) show that an accurate estimation of the phase shift is not easy to produce because it depends on the way the measurement is performed. Therefore, the time displacement was quantified by computing the Fourier decomposition of $h(t, 0)$ and $\gamma(t, 0)$ over time and by measuring the temporal phase shift between the evolutions of the respective dominant modes. That is,

$$h(t,0) = H_0 + \sum_{m=1}^{\infty} H_m(0)\cos(m\pi t), \quad \gamma(t,0) = \Gamma_0 + \sum_{m=1}^{\infty} \Gamma_m(0)\cos(m\pi t). \tag{13}$$

In all the cases presented in this paper, the dominant mode has a frequency equal to $1/2$; consequently, we assume that the phase shift between H_1 and Γ_1 is a reasonable measure of the actual time displacement between $h(t, 0)$ and $\gamma(t, 0)$.

This analysis was done for all the unstable points shown in figure 5 and the results obtained are illustrated in figure 10. We observe that the phase shift rapidly increases with the elasticity number when this parameter is smaller than one, and that it is less affected by β when this number is increased beyond one. That is, the behaviour of the phase shift with β is similar to the behaviour of F (see figure 5), even though the phase shift increases and F diminishes for $\beta > 1$.

The previously reported results corresponding to the evolution of the interfacial variables for $\beta \geqslant 1$ show that an increase of this parameter produces an interfacial distribution of surfactant closer to the initial one, and that the magnitude of the tangential stresses remains similar. Consequently, the Marangoni effect associated with the tangential stresses does not vary significantly for $\beta \geqslant 1$. If the elastic effects $(\mathrm{d}\overline{\sigma}/\mathrm{d}s)$ are fairly constant, a similar behaviour would be expected for both the phase shift and the amplitude of the external acceleration needed to produce the wavy interface. Figures 5 and 10 indicate that these two variables are closely related in the whole range of β considered.

4.4. *The evolution of the flow fields, the interfacial concentration and the Marangoni stresses for selected values of* β

The numerical methodology employed in this work to solve the complete set of governing equations and boundary conditions allows a detailed analysis of the flow fields. Figure 11(*a–c*) illustrates the evolution of the streamlines during a complete cycle of the forcing acceleration for three of the cases close to the threshold conditions considered in §4.2. The streamlines are drawn at regular intervals of approximately 0.1 units of dimensionless time, from $t \approx 198$ to $t \approx 199$, corresponding to the instants identified with dots in figures 6(*f*), 8(*f*), and 9(*f*). The selected cases are: $\beta = 0.2$, $F = 14.25$ (figure 11*a*) $\beta = 1$, $F = 19.5$ (figure 11*b*); $\beta = 3$, $F = 19$ (figure 11*c*). The first three rows in figure 11; show the liquid moving from the left to the right side of the domain; the fourth row approximately corresponds to the instant at which the direction of the motion of the liquid in the bulk is about to be reversed. Finally, the last seven rows depict the fluid flowing from $x = 1$ toward $x = 0$.

In all three cases, the generation of a vortex at the free surface when the liquid is moving toward the right is evident. This vortex is formed due to the Marangoni forces that pull the liquid toward the region in which the concentration of surfactant is lower; that is, in the opposite direction to the flow in the bulk. However, some important differences in the flow fields should be noticed.

As the elasticity grows and the temporal phase shifts become larger (see figure 10), the vortex appears sooner and remains near the interface for longer during the cycle, a fact that can be responsible for an increase of the relative importance of the viscous dissipation (see figure 11*a*, *b*). Moreover, for $\beta = 1$ and $\beta = 3$, the swirls appear, disappear and reappear during the cycle (see figure 11*b*, *c*), a phenomenon that is not observed when $\beta = 0.2$. In these two cases, the flow patterns are very similar and they are in agreement with the changes experienced by the interfacial variables shown in the previous section (figures 8 and 9).

In order to emphasize the interaction that exists between the flow field and the distribution of surfactant, figure 12(*a–c*) depicts the local deviations from the equilibrium value of the concentration of solute adsorbed at the interface, the tangential surface velocity, and the free-surface location, respectively, for the examples presented in figure 11(*a–c*). The curves are numbered consecutively from 1 to 6, in such a way that curve 1 is for the first instant of time considered in figure 11, curve 2 for the third, and so on. The distribution of these variables presents similar characteristics in all three cases, the major difference being the maximum values that depend on the elasticity number.

When the liquid in the bulk phase moves from the left to the right (curves 1 and 2 in figure 12), one would expect the surfactant to be convected toward $x = 1$ giving rise to an increment of the concentration of surfactant there and a diminution at $x = 0$. However, in the three cases analysed, the interfacial velocity changes sign and the

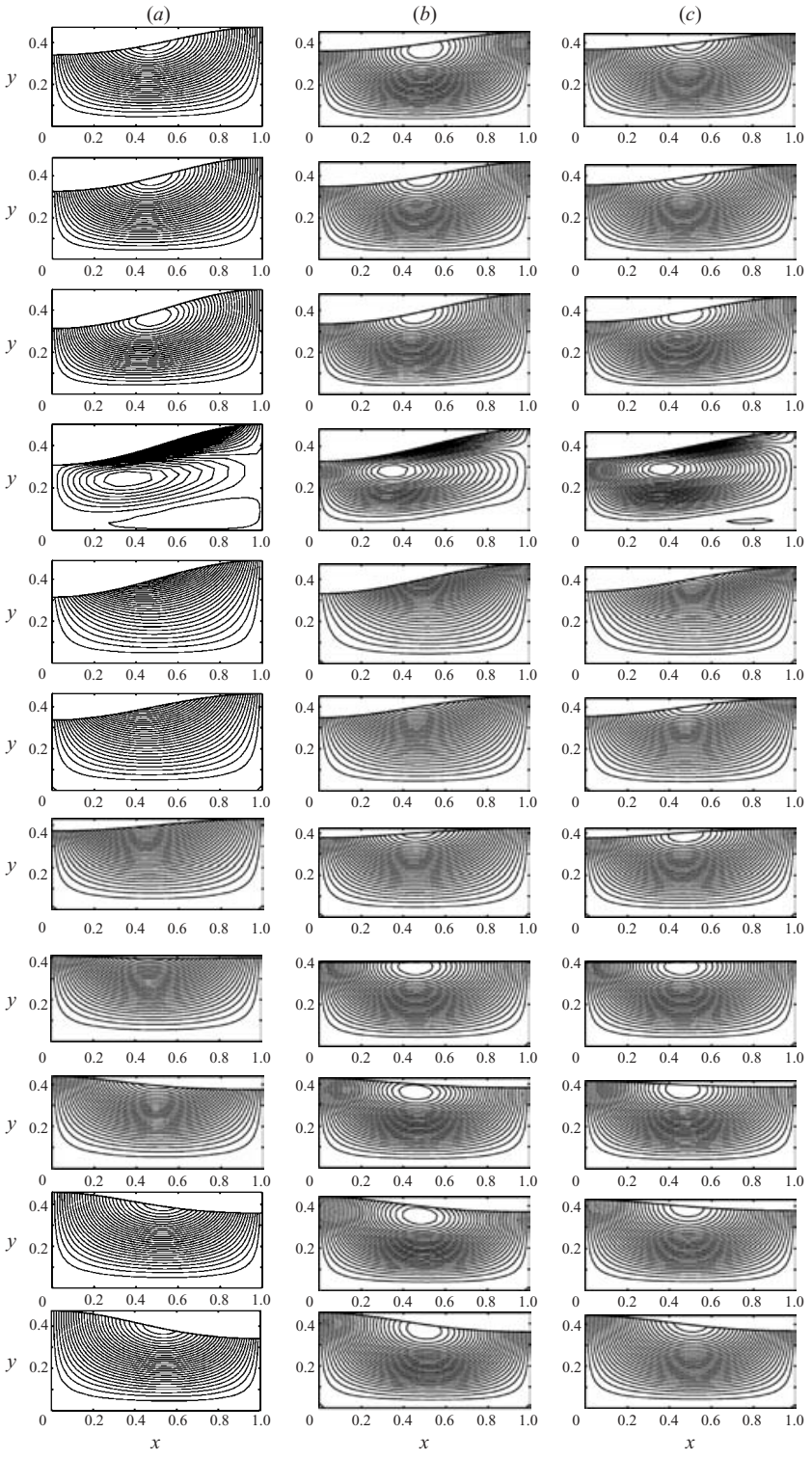

FIGURE 11. Sequence of streamlines for approximately one cycle of the forcing acceleration, for RS, $\alpha = 1.26$. Time advances from top to bottom and each column corresponds to the instants of time indicated with dots on figures 6(f), 8(f) and 9(f) for (a) $\beta = 0.2$, (b) $\beta = 1$, and (c) $\beta = 3$, respectively.

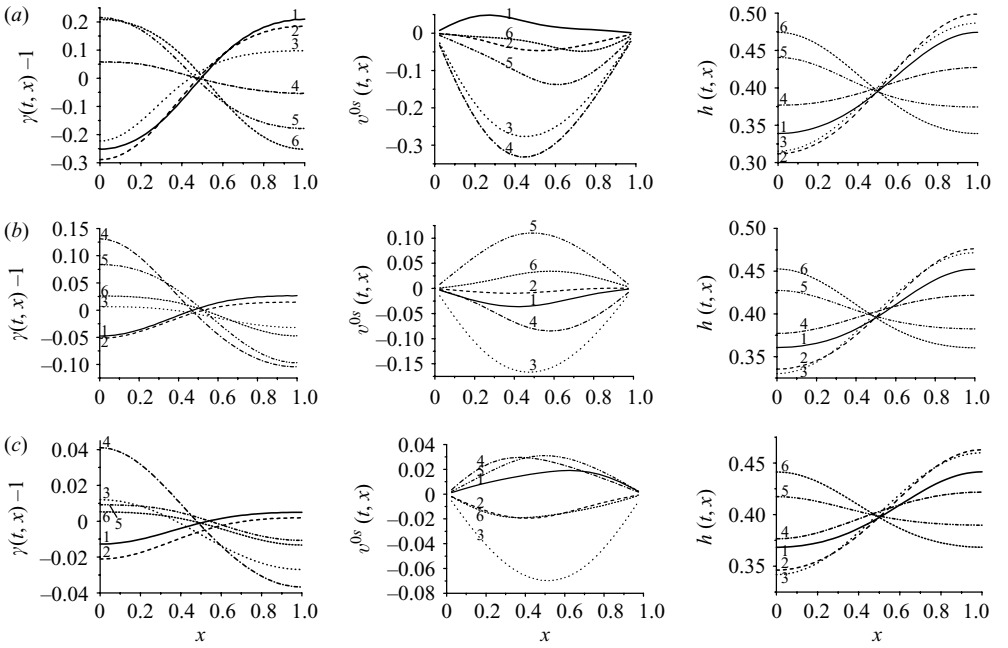

FIGURE 12. Spatial distribution of surfactant concentration departures, interfacial tangential velocity, and free-surface locations for RS, $\alpha = 1.26$. (*a*) $\beta = 0.2$, (*b*) $\beta = 1$, and (*c*) $\beta = 3$. Curves 1 to 6 in each illustration correspond to every other instant of time marked with dots in figures 6*f*, 8*f*, and 9*f*.

direction of convection reverses before the amplitude of the free-surface oscillation achieves its maximum. Consequently, the local concentration of solute diminishes not only at $x = 0$ but also at $x = 1$ throughout this part of the cycle.

When $\beta = 0.2$ and the liquid in the bulk flows from $x = 1$ toward $x = 0$ (curves 3–6 in figure 12*a*), the negative surface velocity convects surfactant in the direction of the liquid motion, creating a positive concentration gradient whose magnitude increases with time. At the last instant illustrated in figure 12(*a*) (almost the mirror image of the first one depicted), the elastic effects are large enough to significantly reduce the tangential surface velocity just before the flow in the bulk reverses.

A different situation is observed during this part of the cycle when β is 1 or 3 (curves 3–6 of figure 12*b*, *c*): the large magnitude of the Marangoni stresses drastically reduces the tangential surface velocity and reverses its direction (see curves 3–6 for v^{0s}) while the liquid in the bulk is still moving from the right to the left of the domain; consequently, the flow of surfactant turns back before the maximum amplitude of the free surface is attained. The maximum value of T_{nt} practically does not change when the elasticity number is varied from 1 to 3; therefore, the interfacial concentration gradient should be about three times smaller when $\beta = 3$ (equations (4) and (5)). This is just the case shown in figure 12(*b*, *c*).

The large tangential stresses generated when the elasticity number is 1 or 3, should drastically reduce the motion of the system near the interface. This effect, combined with a larger temporal shift with respect to the interfacial motion, might produce the two vortices observed in figure 11(*b*, *c*).

In order to gain more insight into the relative significance of the different terms involved in equation (7), we evaluated the contribution to the local concentration of

surfactant of surface convection ($\gamma \mathrm{d}v^{0s}/\mathrm{d}s + v^{0s}\mathrm{d}\gamma/\mathrm{d}s$), surface dilation ($2Hv^{0n}$) and surface diffusion ($Pe^{-1}\,\mathrm{d}^2\gamma/\mathrm{d}s^2$). We did this for the examples illustrated in figure 11(*a–c*), and the results obtained are depicted in figure 13(*a–c*) where numbers on the curves have the same meaning as in figure 12.

It is easy to see that the local concentration of surfactant is mainly affected by convection, which mostly depends on the gradients of surface velocity, and that the diffusive process has a negligible effect on γ during the whole cycle for the three values of β considered. The results also show that the magnitude of the dilation–contraction mechanism ($2Hv^{0n}$) is almost independent of the elasticity number. Nevertheless, while the convective transport is about 6 times larger for $\beta = 0.2$, this ratio reduces to nearly 5 and 3 for β equal to 1 and 3, respectively. Therefore, the reduction of the term ($\gamma \mathrm{d}v^{0s}/\mathrm{d}s$) is responsible for the more uniform distribution of solute that exists along the interface when the elasticity number is increased (see figure 12).

4.5. *The phase shift when* $Pe = 1$

When the Péclet number is large, the phase displacement that exists between the interfacial concentration of the surfactant and the free-surface deflections is closely related to the phase shift that exists between the time evolutions of the interfacial velocities and the flow of the liquid in the bulk. That is, when convection dominates, the elastic effects arising from a non-uniform distribution of solute affect the interfacial velocity in an attempt to reduce the concentration gradients. Then, it is interesting to investigate if there exists a temporal phase shift when diffusion is large enough to counterbalance the effects of convection.

With this purpose we carried out a numerical experiment in which all the characteristic numbers had the values of the reference case, except for Pe which was fixed at 1 and the elasticity number which was set equal to 0.2. Under these conditions, the minimum acceleration needed to form a wavy interface requires a value of F near 13; that is between 11.9 ($\beta = 0$) and 14.25 ($\beta = 0.2$, $Pe = 248667$), as expected.

Although the figures are not shown here, we have calculated the time evolutions of the maximum absolute value of the tangential and normal components of both the surface velocity and surface traction, the surfactant concentration departure from equilibrium, and the free-surface location at the ends of the domain. A comparison between these curves and those illustrated in figure 6 for $Pe = 248\,667$ and $\beta = 0.2$, shows that T_{nt} and γ are the more sensitive variables to the change in the Péclet number. When diffusion is as important as convection ($Pe = 1$), the interfacial distribution of surfactant is very close to the initial concentration during the complete cycle. This more homogeneous distribution of the adsorbed solute gives rise to lower values of the Marangoni stress.

Another important difference detected when results for the two values of Pe are compared is related to the phase shift. In fact, for $Pe = 248667$ and $\beta = 0.2$ there are small temporal phase displacements between the evolution of the motion of the liquid in the bulk and the evolutions of both the tangential velocity of the free surface and the interfacial concentration of surfactant. On the other hand, for $Pe = 1$ and $\beta = 0.2$, the flow in the bulk and along the free surface are almost synchronized, but there is a temporal displacement of about 0.44 units of dimensionless time between the evolutions of the interfacial concentration of solute and the motion in the bulk.

When $Pe = 1$ and the interfacial velocity is large, the concentration of surfactant increases at the end of the domain toward which the liquid is flowing and diminishes at the opposite end. Nevertheless, when the concentration gradient becomes large, the convective transport is not enough to counterbalance the effects of diffusion, and

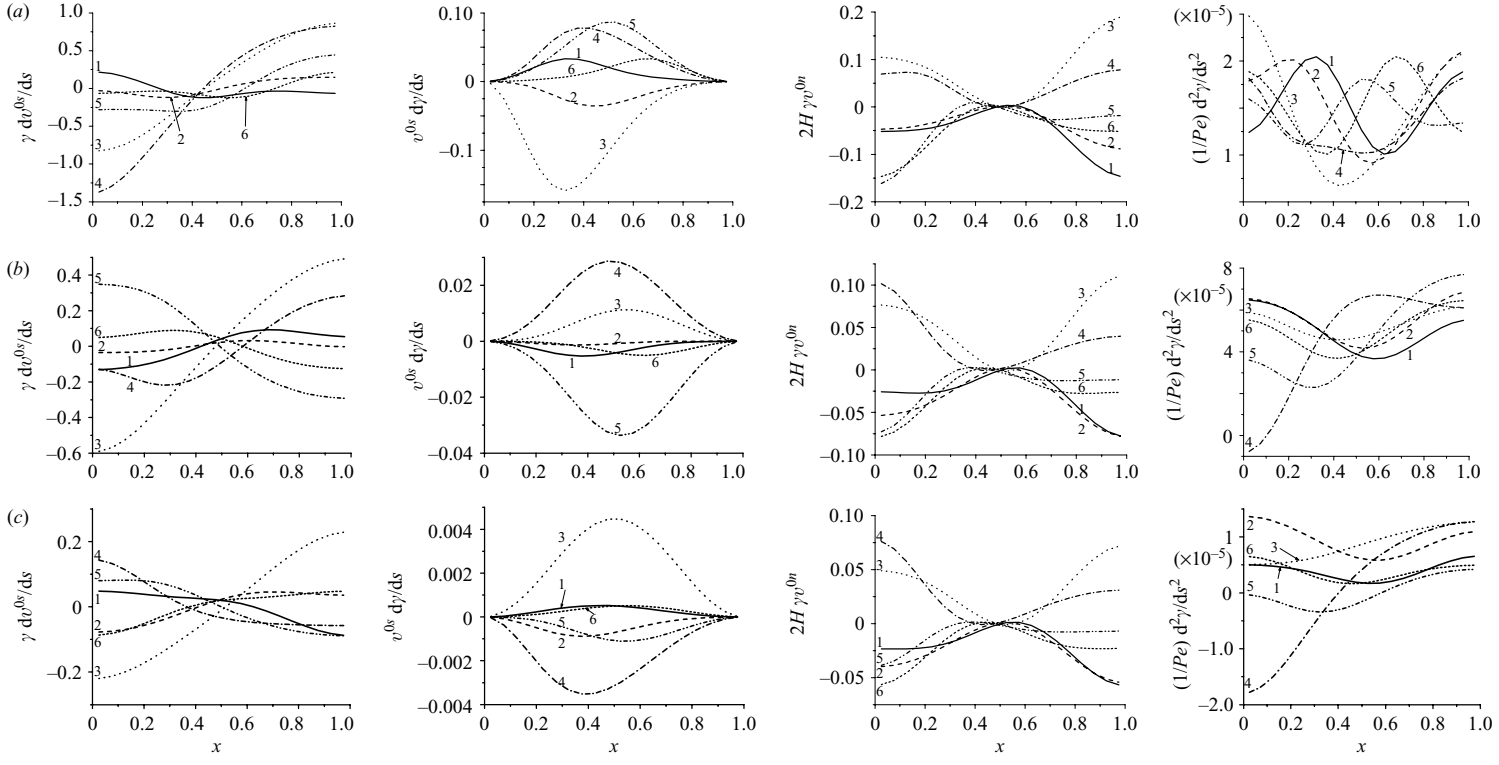

FIGURE 13. Contribution of the local concentration of surfactant to the different terms involved in equation (7) for RS, $\alpha = 1.26$. (*a*) $\beta = 0.2$, (*b*) $\beta = 1$, and (*c*) $\beta = 3$. Curves 1 to 6 in each illustration correspond to every other instant of time marked with dots in figures 6(*f*), 8(*f*) and 9(*f*).

the flow of surfactant reverses sooner than the free-surface shape. This gives rise to the spatial phase shift observed between the evolution of the surfactant concentration and the free-surface deflection.

5. Concluding remarks

In this work we analyse the Faraday instability phenomenon when insoluble surfactants are present. We restricted our analysis to two-dimensional waves and, for each time step, the complete nonlinear set of governing equations was simultaneously solved.

The numerical method employed, which uses the Galerkin/finite element technique coupled with a suitable parameterization of the free surface for the spatial discretization, and a second-order predictor–corrector scheme to march in time, proved to be well suited for our purposes.

The main objective was to examine the influence of the elasticity of the surfactant on the stability of the system; to this end we chose a reference case defined by typical values of the variables involved. Then, numerical experiments were performed for several values of the elasticity number (β); in these experiments the force applied to the oscillatory system was finely tuned to approach, as closely as possible, a state in which two-dimensional standing waves of a predetermined wavelength can be observed. At this point the evolution of different variables such as free-surface location, normal and tangential components of both interfacial velocities and stresses at the interface and surfactant distribution, were examined throughout a complete oscillatory cycle.

The results obtained indicate that for elasticity numbers smaller than a certain value (1 for the case we scrutinized) the system becomes more stable, and larger amplitudes of the forced oscillations, i.e. larger applied forces, were needed to form a wavy interface as β increases. However, this trend is reversed when the elasticity number is larger than one and the force needed to produce standing waves slightly decreases as β becomes larger. From another point of view, one may say that the damping effect of surfactants increases with the elasticity number until certain point beyond which further increases in β will not produce significant effects.

The results also show that the damping effects are originated in the tangential interfacial stresses that induce a temporal phase shift between the evolution of the standing waves and the evolution of the interfacial concentration of surfactant. This phase shift changes with the elasticity number in a rather similar way to the changes of the applied forces just described, although it increases monotonically with β.

The flow fields were visualized by plotting the streamlines for different steps of the cycle; those figures clearly show the vortices appearing at the interface and moving into the bulk before disappearing. This process of vortex formation and vanishing is favoured for larger values of the elasticity number.

The case studied, which was selected by considering typical values of the physical properties and parameters of the system, presents a rather large Péclet number suggesting that convection is the main mechanism of mass transport. This feature was confirmed when the contribution of the different terms in the surfactant equation was analysed.

Finally, with the purpose of illuminating the role of diffusion in this problem, the hypothetical case of $Pe = 1$ and $\beta = 0.2$ was examined. As one would expect the system turns out to be more unstable than the base case with the same value of the elasticity number since diffusion smooths out the concentration gradients produced by convection. Then, a smaller applied force ($F \approx 13$) than in the equivalent base case

($F = 14.25$) is needed to produce the wavy interface. A detailed examination of the variables shows that large diffusion effects induce a noticeable temporal phase shift between the evolutions of the bulk flow and those of the interfacial concentration gradients.

This work has been supported by the Universidad Nacional del Litoral, CONICET and ANPCYT.

REFERENCES

Benjamin, T. B. & Ursell, F. 1954 The stability of the plane free surface of a liquid in a vertical periodic motion. *Proc. R. Soc. Lond.* A **225**, 505.

Faraday, M. 1831 On the forms and states assumed by fluids in contact with vibrating elastic surfaces. *Phil. Trans. R. Soc. Lond.* **121**, 319.

Franklin, B. 1774 On the stilling of waves by means of oil. *Phil. Trans. R. Soc. Lond.* **2**, 144.

Gresho, P. M., Lee, R. L. & Sani, R. L. 1979 On the time-dependent solution of the incompressible Navier-Stokes equations in two and three dimensions. In *Recent Advances in Numerical Methods in Fluids* (ed. C. Taylor & K. Morgan), Vol. 1, Chap. 2, pp. 27. Pineridge Press, Swansea.

Henderson, D. 1998 Effects of surfactants on Faraday-wave dynamics. *J. Fluid Mech.* **365**, 89.

Kheshgi, H. S. & Scriven, L. E. 1984 Penalty finite element analysis of unsteady free surface flows. In *Finite Elements in Fluids* (ed. R. H. Gallagher & J. T. Oden), Vol. 5, Chap. 19, pp. 393, John Wiley & Sons.

Kumar, K. & Tuckerman, L. 1994 Parametric instability of the interface between two fluids. *J. Fluid Mech.* **279**, 49.

Kumar, S. & Matar, O. K. 2002*a* Parametrically driven surface waves in surfactant-covered liquids. *Proc. R. Soc. Lond.* A **458**, 2815.

Kumar, S. & Matar, O. K. 2002*b* Instability of long-wavelength disturbances on gravity-modulated surfactant-covered thin liquid layers. *J. Fluid Mech.* **466**, 249.

Lamb, H. 1945 *Hydrodynamics*. Dover.

Miles, J. 1967 Surface wave damping in closed basins. *Proc. R. Soc. Lond.* A **297**, 459.

Miles, J. & Henderson, D. 1990 Parametrically forced surface waves. *Annu. Rev. Fluid Mech.* **22**, 143.

Stone, H. A. 1990 A simple derivation of the time-dependent convective-diffusive transport equation for surfactant transport along a deforming interface. *Phys. Fluids* A **2**, 111.

Ubal, S. 2002 Estudio de la influencia del espesor del líquido y de los surfactantes sobre las ondas de Faraday bidimensionales. Análisis numérico. Doctoral thesis, Universidad Nacional del Litoral.

Ubal, S., Giavedoni, M. D. & Saita, F. A. 2003 A numerical analysis of the influence of the liquid depth on two dimensional Faraday waves *Phys. Fluids* **15**, 3099.

Wong, H., Rumschitzki, D. & Maldarelli, C. 1996 On the surfactant mass balance at a deforming fluid interface. *Phys. Fluids* **8**, 3203.